Charge carrier dynamics of FeSe thin film investigated by terahertz magneto-optical spectroscopy

Naotaka Yoshikawa,[1] Masayuki Takayama,[1] Naoki Shikama,[2] Tomoya Ishikawa,[2] Fuyuki Nabeshima,[2] Atsutaka Maeda,[2] and Ryo Shimano[1,3]

[1]*Department of Physics, The University of Tokyo, Hongo, Tokyo 113-0033, Japan*
[2]*Department of Basic Science, The University of Tokyo, Meguro, Tokyo 153–8902, Japan*
[3]*Cryogenic Research Center, The University of Tokyo, Yayoi, Tokyo 113-0032, Japan*

(Received 16 February 2019; revised manuscript received 12 May 2019; published 12 July 2019)

We performed terahertz magneto-optical spectroscopy of FeSe thin film to elucidate the charge carrier dynamics. The measured diagonal (longitudinal) and off-diagonal (Hall) conductivity spectra are well reproduced by a two-carrier Drude model, from which the carrier densities, scattering times, and effective masses of electron and hole carriers are determined in a wide range of temperature. The hole density decreases below the structural transition temperature while electron density increases, which is attributed to the band-structure modification in the electronic nematic phase. The scattering time of the hole carrier becomes substantially longer than that of the electron at lower temperature, which accounts for the increase of the positive dc Hall coefficient at low temperature.

DOI: 10.1103/PhysRevB.100.035110

I. INTRODUCTION

Since the discovery of iron-based superconductors (FeSCs), tremendous research efforts have been devoted to reveal the pairing mechanism of superconductivity. The elucidation of interplay between the nematic order, antiferromagnetic spin order, and superconductivity emergent in FeSCs has been believed to provide a clue to understand the emergent superconductivity. Among FeSCs, FeSe provides a unique playground to study the role of nematicity, because it lacks the long-range magnetic order in the nematic phase that appears below the tetragonal-orthorhombic structural transition temperature $T_s \approx 90$ K, as evidenced by a significant electronic anisotropy from transport and NMR spectral properties [1–3]. While the superconducting transition temperature T_c of bulk FeSe is ∼9 K at ambient pressure [4], it shows a remarkable tunability. T_c increases to as high as 38 K under hydrostatic pressure [5–8], and single-layer FeSe grown on $SrTiO_3$ shows T_c up to 109 K [9–11]. Electron doping by ionic gating in FeSe thin flakes enhances the superconductivity toward 48 K [12–15]. Intercalation also enhances T_c by a similar doping effect in addition to an effect of separating the layers [16]. One important key to understand the T_c increase of FeSe is considered to be a change of the Fermi-surface topology. The high tunability of the electronic structure of FeSe achieved by various ways is related to its extremely small effective Fermi energy (∼10 meV), which has been demonstrated in FeSe [17] as well as $FeSe_{1-x}Te_x$ [18,19]. FeSe is a semimetal with the Fermi surface consisting of hole pockets around the Brillouin-zone center Γ point and electron pockets around the zone corner M point. The low-energy electronic structure around the Fermi level has been experimentally revealed by angle-resolved photoemission spectroscopy (ARPES) [20–24]. ARPES studies have also shown a significant modification of the band structure below T_s which is attributed to the development of an electronic nematicity.

For the understanding of unconventional superconductivity in FeSe, it is also indispensable to investigate the charge carrier dynamics in normal and nematic phases as well as in superconducting phase. The Hall resistivity measured by magnetotransport shows an unusual temperature dependence with the sign change owing to the nearly compensated electron and hole carriers [17,25–27]. In bulk FeSe, the presence of a small number of highly mobile electronlike carrier at the nematic phase was also identified by the Hall resistivity [25] and mobility spectrum analysis [28], which could be attributed to the Dirac-like dispersion near the M point [29]. However, the complexity of the multiband Fermi surfaces of FeSe makes it difficult to grasp the properties of charge carriers only by dc transport measurements. This is because the characterization of the carriers by dc transport measurements needs to assume some models such as a compensated two-band model, where the compensated electron is assumed to have the same carrier density as that of the hole ($n_e = n_h$) [25,27,28,30]. Although a three-band model can also be used by including the nonlinear term when dc transport is measured up to high magnetic field, the characterization is not complete because the mobility, which is determined by dc transport in addition to carrier densities, is a function of effective mass and scattering time. For more detailed characterization of charge carriers, quantum oscillations are a well-established technique [22,25,31,32]. However, there is a prerequest for the observation of quantum oscillations that the sample should have high mobility electrons, which has restricted the measurements at very low temperature in bulk single crystals. Therefore, the independent determination of the properties of charge carriers of FeSe in a wide range of temperature in particular across the structural phase transition has been lacked. It has remained

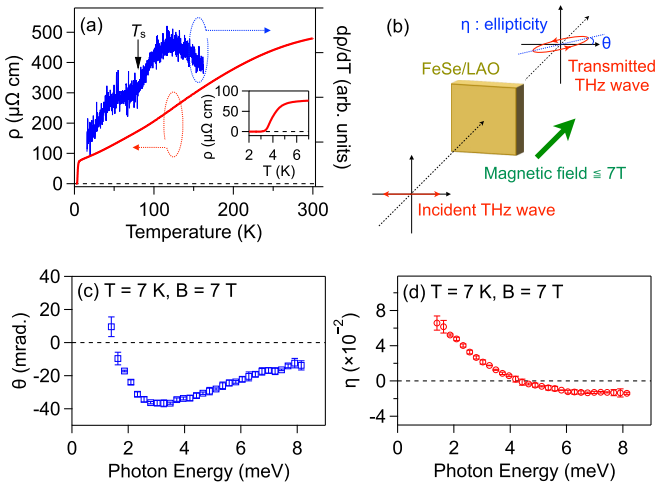

FIG. 1. (a) Temperature dependence of dc resistivity ρ (red line) and $d\rho/dT$ (blue line) of the FeSe thin film. A kink anomaly at T_s is indicated by black arrow. Inset shows an enlarged view of the resistivity curve around $T_c \sim 3$ K. (b) Schematic of our THz magnetospectroscopy. (c) Faraday rotation spectrum and (d) ellipticity spectrum induced by FeSe film at 7 K with the magnetic field of 7 T.

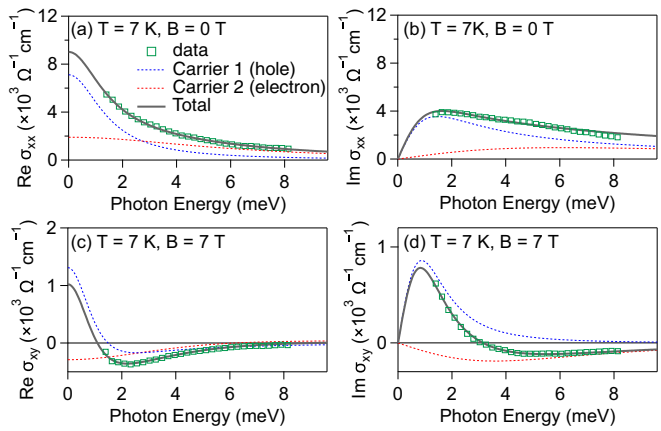

FIG. 2. (a) Real- and (b) imaginary part of the longitudinal optical conductivity spectrum, and (c) real- and (d) imaginary part of the optical Hall conductivity spectrum, respectively, of FeSe at $T = 7$ K with $B = 7$ T. Green open square represents experimental result, blue dashed, red dashed, and gray solid line indicate, respectively, the contribution of the hole carrier, electron carrier, and sum of them given by the two-carrier Drude fitting described in the text.

to be clarified how the nematicity affects the charge carrier properties of FeSe.

In this study, we investigate the charge dynamics in a thin-film FeSe by terahertz (THz) magneto-optical spectroscopy. The obtained diagonal (longitudinal) and off-diagonal (Hall) conductivity spectra are well described by a two-carrier Drude model, from which the carrier densities, scattering times, and effective masses of electron and hole carriers were independently determined. The temperature dependence of THz magneto-optical spectra revealed the significant change of the carrier densities below T_s, which is plausibly attributed to the band-structure modification in the nematic phase. The scattering time of the hole carrier substantially increases at lower temperature, which explains the peculiar temperature dependence of the dc Hall coefficient in FeSe thin films.

II. EXPERIMENT

An FeSe thin film with the thickness of 46 nm was fabricated on $LaAlO_3$ (LAO) substrate by the pulsed-laser deposition method [33,34]. The temperature dependence of dc resistivity shows the superconducting transition at $T_c \sim 3$ K defined by the zero resistivity [Fig. 1(a)]. A kink anomaly in $d\rho/dT$ curve indicates the structural transition at $T_s \sim 80$ K. Figure 1(b) shows the schematic of our THz magneto-spectroscopy based on THz time-domain spectroscopy (THz-TDS) [35–37]. The output of a mode-locked Ti:sapphire laser with the pulse duration of 110 fs, center wavelength of 800 nm, and repetition rate of 76 MHz was focused onto a p-type (111) InAs surface to generate THz pulses. Linearly polarized THz incident pulses were focused on the sample placed in a split-type superconducting magnet which can produce the magnetic field up to 7 T in Faraday configuration, that is, the magnetic field is parallel to the wave vector of the THz wave. The THz wave was detected by electro-optical sampling with a (110) ZnTe crystal. By measuring the waveform of the parallel polarization component defined as $E_x(t)$ and perpendicular polarization component $E_y(t)$ of the transmitted THz pulses by using wire-grid polarizers, the Faraday rotation angle θ and ellipticity η induced by the FeSe film in the magnetic field can be obtained. Here, the approximated expression $\frac{E_y(\omega)}{E_x(\omega)} \sim \theta(\omega) + i\eta(\omega)$ for small Faraday rotation angle was used. Figures 1(c) and 1(d) show the THz Faraday rotation angle and ellipticity, respectively, under $B = 7$ T at the sample temperature $T = 7$ K. The error bars indicate the standard deviations determined by the multiple measurements, confirming that the obtained signal $\theta(\omega)$ and $\eta(\omega)$ well exceeds the noise level.

III. RESULTS

A. Properties of the charge carriers

Figures 2(a) and 2(b) show the real- and imaginary part of the longitudinal optical conductivity spectrum $\sigma_{xx}(\omega)$ of FeSe at 7 K, respectively, given by the normal transmission type THz-TDS without magnetic field. The combination of the obtained $\sigma_{xx}(\omega)$, $\theta(\omega)$, and $\eta(\omega)$ provides the optical Hall conductivity spectrum $\sigma_{xy}(\omega)$ through the following equation for a thin film under small rotation angle approximations:

$$\theta + i\eta \sim \frac{1}{\left(1 + n_{\mathrm{sub}}(\omega) - \frac{i\omega d n_{\mathrm{sub}}(\omega)}{c}\right)c\varepsilon_0 + \sigma_{xx}(\omega)d}\sigma_{xy}(\omega)d, \tag{1}$$

where n_{sub} is the refractive index of the substrate, d the thickness of FeSe film, c speed of light, and ε_0 permittivity of vacuum. Figures 2(c) and 2(d) show the real- and imaginary part of the optical Hall conductivity spectrum with $B = 7$ T, respectively. The data set of the complex longitudinal and Hall

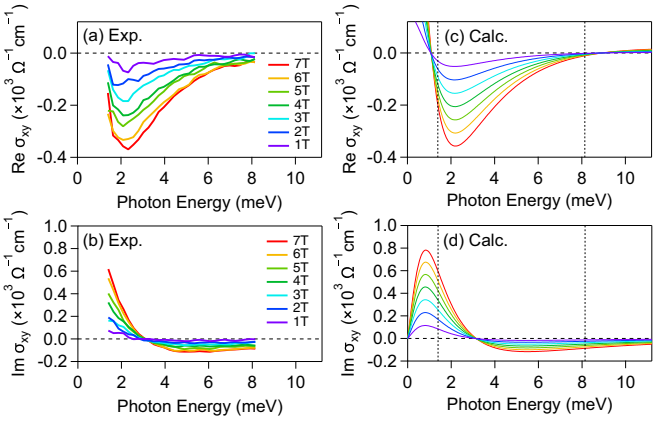

FIG. 3. (a) Real- and (b) imaginary part of the optical Hall conductivity spectrum with various magnetic-field strength of 1–7 T. (c), (d) Magnetic-field dependence of calculated curves by the two-carrier Drude model. Dashed vertical lines indicate the spectral range of the experiment.

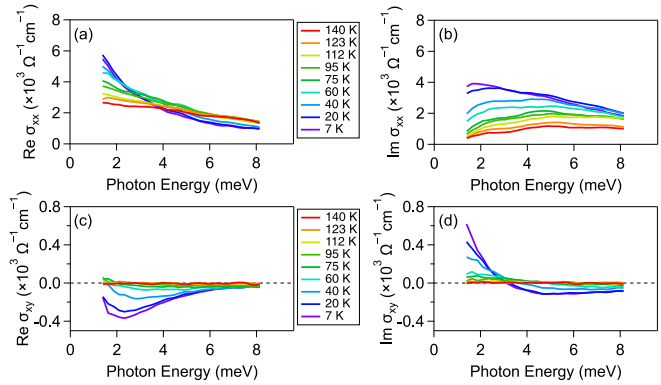

FIG. 4. Temperature dependence of (a) real- and (b) imaginary part of the longitudinal optical conductivity, and (c) real- and (d) imaginary part of the optical Hall conductivity of FeSe thin film with $B = 7$ T.

conductivity spectra was well fitted by the Drude model with an electron carrier and a hole carrier:

$$\sigma_{xx}(\omega, B=0) = \frac{n_e {q_e}^2 \tau_e}{m_e^*} \frac{1}{1 - i\omega\tau_e} + \frac{n_h {q_h}^2 \tau_h}{m_h^*} \frac{1}{1 - i\omega\tau_h}, \quad (2)$$

$$\sigma_{xy}(\omega, B) = \frac{n_e {q_e}^2 \tau_e}{m_e^*} \frac{\omega_{c,e}\tau_e}{(1 - i\omega\tau_e)^2 - {\omega_{c,e}}^2} + \frac{n_h {q_h}^2 \tau_h}{m_h^*} \frac{\omega_{c,h}\tau_h}{(1 - i\omega\tau_h)^2 - {\omega_{c,h}}^2}, \quad (3)$$

where $q_e = -e$ ($q_h = +e$), n_e (n_h), τ_e (τ_h), m_e^* (m_h^*), $\omega_{c,e} = q_e B/m_e^*$ ($\omega_{c,h} = q_h B/m_h^*$) represent the charge of carrier, carrier density, scattering time, effective mass, and cyclotron frequency of the electrons (holes), respectively. Notably, the optical Hall conductivity is sensitive to the carrier type (electronlike or holelike) while the longitudinal conductivity is formally independent of the sign of the charge carriers. The sign change around 3 meV in the imaginary part of $\sigma_{xy}(\omega)$ indicates that two types of carriers exist with different sign of charge, which can be attributed to those in the electron pocket and hole pocket in FeSe. We can determine the complete set of the parameters describing charge carrier dynamics, $n_e = 5.4 \times 10^{19}$ cm^{-3}, $n_h = 1.7 \times 10^{20}$ cm^{-3}, $m_e = 0.86 m_0$, $m_h = 2.90 m_0$, $\tau_e = 0.11$ ps, and $\tau_h = 0.45$ ps. We also checked the magnetic-field dependence of the complex optical Hall conductivity. Figures 3(a) and 3(b) show the real- and imaginary part of the complex optical Hall conductivities at 7 K with various magnetic fields, and Figs. 3(c) and 3(d) show those given by the Drude model with various B in Eq. (3) and the fixed other parameters. The good agreement of the experimental data and two-carrier Drude model validates the interpretation that the THz conductivity spectra are mainly contributed by two charge carriers (electrons and holes). The effective mass of the hole evaluated by quantum oscillation and ARPES studies are typically around $4m_0$, which is consistent with our result [22,31,32,38]. The effective mass of the electron, on the other hand, differs among various reports. The present THz magneto-spectroscopy shows the similar effective mass with that deduced by the band curvature measured by ARPES [38,39]. The carrier densities n_e and n_h are also reasonable compared with the various transport measurements [25,27,28]. The ARPES measurements showed that the Fermi surface around the zone center consists of the outer and inner hole pockets above the structural transition temperature, while the inner hole pocket moves completely below the Fermi level in the nematic phase [22]. Thus, the carrier density and effective mass of the hole at 7 K evaluated by the THz magnetospectroscopy are most likely attributed to that of the outer hole pocket. On the other hand, the Fermi surface around the M point consists of at least two electron pockets in the nematic phase. Here the electrons in the outer electron pocket are considered to contribute dominantly to the transport and charge dynamics, so the obtained parameters of the electron are probably those of the outer electron pocket. It should be noted here that the wavelength of THz probe is on the order of 100 μm, and correspondingly the wave number q is negligibly small. In such a $q = 0$ limit, it is known that the Drude model can be applied even though the effective Fermi energy is small and comparable with the probe photon energy ($\hbar\omega \sim E_F$) [40].

B. Temperature dependence

Next, we investigated the temperature dependence of conductivity spectra. Figures 4(a) and 4(b) show the complex longitudinal optical conductivity spectra from 7 to 140 K. The conductivity spectrum shows a broadening at higher temperature indicating the shorter scattering time of the carriers. The optical Hall conductivity spectra in Figs. 4(c) and 4(d) show more notable change where it goes to almost zero at 140 K. We performed the two-carrier Drude fitting as done in Fig. 2 for various temperatures and extracted the parameters describing the observed complex conductivity spectra. Here we fixed effective masses of the electron and hole to those obtained for 7 K. From the fitting, we elucidate that zero Hall conductivity in the THz frequency at 140 K is a consequence of almost completely compensated electron and hole carriers at this temperature (Fig. 5). Figure 6 summarizes

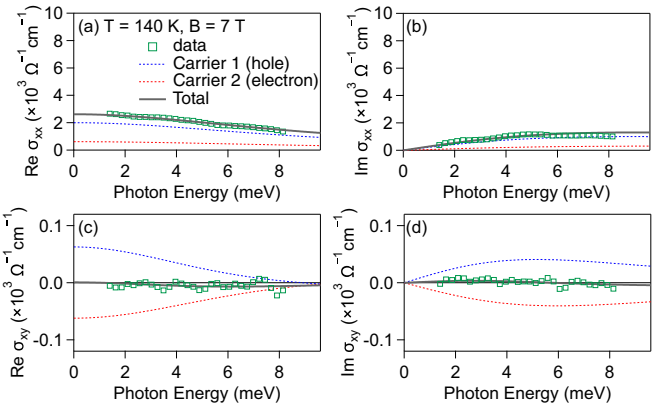

FIG. 5. (a) Real- and (b) imaginary part of the longitudinal optical conductivity spectrum, and (c) real- and (d) imaginary part of the optical Hall conductivity spectrum, respectively, of FeSe at $T = 140$ K with $B = 7$ T. Green open squares represent the experimental data. Blue dashed, red dashed, and black solid lines show, respectively, the contribution of the hole carrier, electron carrier, and sum of them given by the two-carrier Drude fitting.

the temperature dependence of the extracted charge carrier parameters. The scattering time of the hole is shortened at higher temperature while that of the electron weakly depends on the temperature as shown in Fig. 6(a). By considering that the impurity scattering dominates at $T = 0$ limit, it is found that the impurity scattering rate of the electron is larger than that of the hole. This could be derived from the about three times lighter effective mass of the electron than the hole. Since the ARPES measurements revealed that the Fermi wave numbers k_F of the electron and the hole pockets

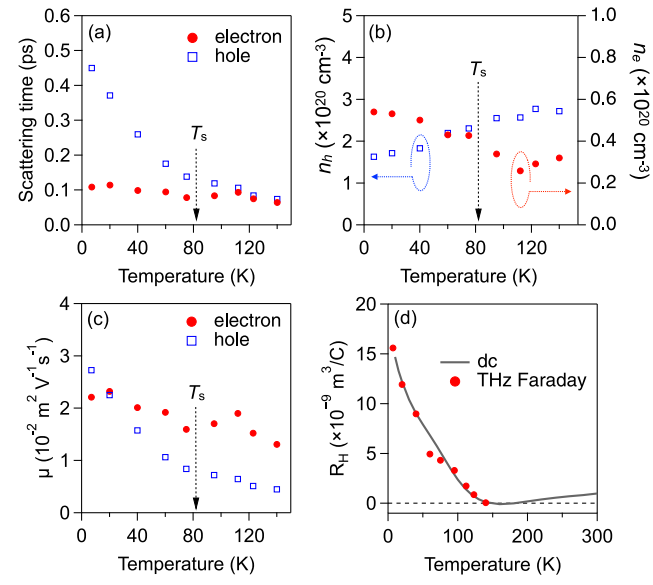

FIG. 6. Temperature dependence of (a) scattering times, (b) carrier densities, (c) mobilities of the electron and hole of FeSe thin film given by THz magnetospectroscopy. The structural transition temperature T_s is indicated by arrows. (d) Hall coefficient of FeSe thin film as a function of temperature, obtained by THz magnetospectroscopy (red circles) and dc transport measurement (gray line).

are similar to each other [20–22,38,39], the Fermi velocity $v_F = k_F/m^*$ of the electron is larger than that of the hole. The carrier with the larger Fermi velocity is expected to have the larger scattering rate with the impurities with certain density. Concomitantly, the hole density substantially reduces at lower temperature below T_s while that of electrons increases. These behaviors seem to correlate with the band-structure change between tetragonal and orthorhombic phase accompanied by electronic nematicity. As for the hole pockets around the Γ point, the ARPES revealed that the inner hole band moves below the Fermi energy in the nematic phase [22], leading to the smaller hole carrier density. The d_{xy} band which forms the outer electron pocket at the M point is also pushed down with decreasing temperature, resulting in the increase of electron density at lower temperature below T_s. A decrease of carrier densities below the structural transition temperature has been observed in bulk FeSe by the dc magnetotransport measurement [25]. The strong anisotropy of the scattering rate induced by the enhancement of spin fluctuations below T_s was suggested to explain the drop of the *effective* electron and hole densities without a change of Fermi-surface volume. However, our observation of the simultaneous increase of the hole density and decrease of the electron density cannot be explained only by the strongly anisotropic carrier scattering. The present THz magneto-optical spectroscopy unambiguously reveals the temperature dependence of the electron and hole densities, which suggests the Fermi-surface modification in the nematic phase. The reduction of carrier density below T_s has also been observed by conventional far-infrared optical reflectivity measurement [41]. By using the scattering time and effective mass, we further evaluate the mobility $\mu = e\tau/m^*$ for each carrier as shown in Fig. 6(c). The mobility of the hole increases at lower temperature as a result of the increase of the scattering time. The temperature dependence of the dc Hall coefficient described as $R_H \approx \frac{\sigma_{xy}(\omega=0)}{\sigma_{xx}(\omega=0)^2 B}$ is plotted (red circles) in Fig. 6(d). We also show the dc Hall coefficient of an FeSe film which was fabricated exactly in a same manner as that used for the THz measurements (gray solid curve), showing the same T_c. The dc Hall effect was measured by a conventional four-probe method with a film fabricated in a six-terminal shape using a metal mask [42]. They show an excellent agreement with each other, indicating that the dc transport and the THz response are described by the common physical origin of the charge carrier dynamics. Accordingly, the peculiar temperature dependence of the Hall coefficient that increases monotonically toward the low temperature is dominantly attributed to the increase of hole scattering time.

IV. CONCLUSION

In summary, we performed THz magneto-optical spectroscopy to investigate the charge carrier dynamics in FeSe. The obtained diagonal and off-diagonal conductivity spectra are well described by a two-carrier Drude model, from which the carrier densities, scattering times, and effective masses of electron and hole carriers are determined in a wide temperature range. We found the significant temperature dependence of the carrier densities of electrons and holes below T_s, which is most likely attributed to the band-structure modification

at the structural phase transition. The scattering time of the hole carrier becomes substantially longer than that of the electron at lower temperature, which results in the positive dc Hall coefficient at low temperature observed in the present FeSe thin film. We demonstrated that THz magneto-optical spectroscopy is a powerful tool for investigating the charge carrier dynamics of FeSe. The application of the technique to FeSe system under pressure, with ionic gating, and thin film or single layer on various substrates would pave a unique pathway to access the charge carrier properties, thereby providing a deep insight into their correlation with the nematicity and the superconductivity.

ACKNOWLEDGMENTS

This work was supported by JSPS KAKENHI (Grants No. 18H05324, No. 18H05846, and No. 18H04212).

[1] T. M. McQueen, A. J. Williams, P. W. Stephens, J. Tao, Y. Zhu, V. Ksenofontov, F. Casper, C. Felser, and R. J. Cava, Phys. Rev. Lett. **103**, 057002 (2009).
[2] S.-H. Baek, D. V. Efremov, J. M. Ok, J. S. Kim, J. van den Brink, and B. Büchner, Nat. Mater. **14**, 210 (2014).
[3] A. E. Böhmer, T. Arai, F. Hardy, T. Hattori, T. Iye, T. Wolf, H. V. Löhneysen, K. Ishida, and C. Meingast, Phys. Rev. Lett. **114**, 027001 (2015).
[4] F.-C. Hsu, J.-Y. Luo, K.-W. Yeh, T.-K. Chen, T.-W. Huang, P. M. Wu, Y.-C. Lee, Y.-L. Huang, Y.-Y. Chu, D.-C. Yan, and M.-K. Wu, Proc. Natl. Acad. Sci. USA **105**, 14262 (2008).
[5] S. Medvedev, T. M. McQueen, I. A. Troyan, T. Palasyuk, M. I. Eremets, R. J. Cava, S. Naghavi, F. Casper, V. Ksenofontov, G. Wortmann, and C. Felser, Nat. Mater. **8**, 630 (2009).
[6] T. Imai, K. Ahilan, F. L. Ning, T. M. McQueen, and R. J. Cava, Phys. Rev. Lett. **102**, 177005 (2009).
[7] Y. Mizuguchi, F. Tomioka, S. Tsuda, T. Yamaguchi, and Y. Takano, Appl. Phys. Lett. **93**, 152505 (2008).
[8] J. P. Sun, K. Matsuura, G. Z. Ye, Y. Mizukami, M. Shimozawa, K. Matsubayashi, M. Yamashita, T. Watashige, S. Kasahara, Y. Matsuda, B. C. Sales, Y. Uwatoko, J. Q. Yan, J. G. Cheng, and T. Shibauchi, Nat. Commun. **7**, 12146 (2016).
[9] J.-F. Ge, Z.-L. Liu, C. Liu, C.-L. Gao, D. Qian, Q.-K. Xue, Y. Liu, and J.-F. Jia, Nat. Mater. **14**, 285 (2014).
[10] S. He, J. He, W. Zhang, L. Zhao, D. Liu, X. Liu, D. Mou, Y.-B. Ou, Q.-Y. Wang, Z. Li, L. Wang, Y. Peng, Y. Liu, C. Chen, L. Yu, G. Liu, X. Dong, J. Zhang, C. Chen, Z. Xu, X. Chen, X. Ma, Q. Xue, and X. J. Zhou, Nat. Mater. **12**, 605 (2013).
[11] S. Tan, Y. Zhang, M. Xia, Z. Ye, F. Chen, X. Xie, R. Peng, D. Xu, Q. Fan, H. Xu, J. Jiang, T. Zhang, X. Lai, T. Xiang, J. Hu, B. Xie, and D. Feng, Nat. Mater. **12**, 634 (2013).
[12] B. Lei, J. H. Cui, Z. J. Xiang, C. Shang, N. Z. Wang, G. J. Ye, X. G. Luo, T. Wu, Z. Sun, and X. H. Chen, Phys. Rev. Lett. **116**, 077002 (2016).
[13] J. Shiogai, Y. Ito, T. Mitsuhashi, T. Nojima, and A. Tsukazaki, Nat. Phys. **12**, 42 (2015).
[14] K. Hanzawa, H. Sato, H. Hiramatsu, T. Kamiya, and H. Hosono, IEEE Trans. Appl. Supercond. **27**, 1 (2017).
[15] S. Kouno, Y. Sato, Y. Katayama, A. Ichinose, D. Asami, F. Nabeshima, Y. Imai, A. Maeda, and K. Ueno, Sci. Rep. **8**, 14731 (2018).
[16] M. Burrard-Lucas, D. G. Free, S. J. Sedlmaier, J. D. Wright, S. J. Cassidy, Y. Hara, A. J. Corkett, T. Lancaster, P. J. Baker, S. J. Blundell, and S. J. Clarke, Nat. Mater. **12**, 15 (2012).
[17] S. Kasahara, T. Watashige, T. Hanaguri, Y. Kohsaka, T. Yamashita, Y. Shimoyama, Y. Mizukami, R. Endo, H. Ikeda, K. Aoyama, T. Terashima, S. Uji, T. Wolf, H. von Löhneysen, T. Shibauchi, and Y. Matsuda, Proc. Natl. Acad. Sci. USA **111**, 16309 (2014).
[18] Y. Lubashevsky, E. Lahoud, K. Chashka, D. Podolsky, and A. Kanigel, Nat. Phys. **8**, 309 (2012).
[19] K. Okazaki, Y. Ito, Y. Ota, Y. Kotani, T. Shimojima, T. Kiss, S. Watanabe, C. T. Chen, S. Niitaka, T. Hanaguri, H. Takagi, A. Chainani, and S. Shin, Sci. Rep. **4**, 4109 (2014).
[20] T. Shimojima, Y. Suzuki, T. Sonobe, A. Nakamura, M. Sakano, J. Omachi, K. Yoshioka, M. Kuwata-Gonokami, K. Ono, H. Kumigashira, A. E. Böhmer, F. Hardy, T. Wolf, C. Meingast, H. v. Löhneysen, H. Ikeda, and K. Ishizaka, Phys. Rev. B **90**, 121111(R) (2014).
[21] P. Zhang, T. Qian, P. Richard, X. P. Wang, H. Miao, B. Q. Lv, B. B. Fu, T. Wolf, C. Meingast, X.-X. Wu, Z. Q. Wang, J. P. Hu, and H. Ding, Phys. Rev. B **91**, 214503 (2015).
[22] M. D. Watson, T. K. Kim, A. A. Haghighirad, N. R. Davies, A. McCollam, A. Narayanan, S. F. Blake, Y. L. Chen, S. Ghannadzadeh, A. J. Schofield, M. Hoesch, C. Meingast, T. Wolf, and A. I. Coldea, Phys. Rev. B **91**, 155106 (2015).
[23] K. Nakayama, Y. Miyata, G. N. Phan, T. Sato, Y. Tanabe, T. Urata, K. Tanigaki, and T. Takahashi, Phys. Rev. Lett. **113**, 237001 (2014).
[24] L. Fanfarillo, J. Mansart, P. Toulemonde, H. Cercellier, P. Le Fèvre, F. Bertran, B. Valenzuela, L. Benfatto, and V. Brouet, Phys. Rev. B **94**, 155138 (2016).
[25] M. D. Watson, T. Yamashita, S. Kasahara, W. Knafo, M. Nardone, J. Béard, F. Hardy, A. McCollam, A. Narayanan, S. F. Blake, T. Wolf, A. A. Haghighirad, C. Meingast, A. J. Schofield, H. von Löhneysen, Y. Matsuda, A. I. Coldea, and T. Shibauchi, Phys. Rev. Lett. **115**, 027006 (2015).
[26] Y. Sun, T. Yamada, S. Pyon, and T. Tamegai, Phys. Rev. B **94**, 134505 (2016).
[27] F. Nabeshima, M. Kawai, T. Ishikawa, N. Shikama, and A. Maeda, Jpn. J. Appl. Phys. **57**, 120314 (2018).
[28] K. K. Huynh, Y. Tanabe, T. Urata, H. Oguro, S. Heguri, K. Watanabe, and K. Tanigaki, Phys. Rev. B **90**, 144516 (2014).
[29] S. Y. Tan, Y. Fang, D. H. Xie, W. Feng, C. H. P. Wen, Q. Song, Q. Y. Chen, W. Zhang, Y. Zhang, L. Z. Luo, B. P. Xie, X. Lai, and D. L. Feng, Phys. Rev. B **93**, 104513 (2016).
[30] Y. A. Ovchenkov, D. A. Chareev, V. A. Kulbachinskii, V. G. Kytin, D. E. Presnov, O. S. Volkova, and A. N. Vasiliev, Supercond. Sci. Technol. **30**, 035017 (2017).
[31] T. Terashima, N. Kikugawa, A. Kiswandhi, E.-S. Choi, J. S. Brooks, S. Kasahara, T. Watashige, H. Ikeda, T. Shibauchi, Y. Matsuda, T. Wolf, A. E. Böhmer, F. Hardy, C. Meingast, H. V. Löhneysen, M.-T. Suzuki, R. Arita, and S. Uji, Phys. Rev. B **90**, 144517 (2014).

[32] A. Audouard, F. Duc, L. Drigo, P. Toulemonde, S. Karlsson, P. Strobel, and A. Sulpice, Europhys. Lett. **109**, 27003 (2015).
[33] Y. Imai, R. Tanaka, T. Akiike, M. Hanawa, I. Tsukada, and A. Maeda, Jpn. J. Appl. Phys. **49**, 023101 (2010).
[34] Y. Imai, T. Akiike, M. Hanawa, I. Tsukada, A. Ichinose, A. Maeda, T. Hikage, T. Kawaguchi, and H. Ikuta, Appl. Phys. Express **3**, 043102 (2010).
[35] Y. Ikebe and R. Shimano, Appl. Phys. Lett. **92**, 012111 (2008).
[36] Y. Ikebe, R. Shimano, M. Ikeda, T. Fukumura, and M. Kawasaki, Phys. Rev. B **79**, 174525 (2009).
[37] R. Shimano, G. Yumoto, J. Y. Yoo, R. Matsunaga, S. Tanabe, H. Hibino, T. Morimoto, and H. Aoki, Nat. Commun. **4**, 1841 (2013).
[38] G. N. Phan, K. Nakayama, K. Sugawara, T. Sato, T. Urata, Y. Tanabe, K. Tanigaki, F. Nabeshima, Y. Imai, A. Maeda, and T. Takahashi, Phys. Rev. B **95**, 224507 (2017).
[39] M. D. Watson, T. K. Kim, L. C. Rhodes, M. Eschrig, M. Hoesch, A. A. Haghighirad, and A. I. Coldea, Phys. Rev. B **94**, 201107(R) (2016).
[40] M. Dressel and G. Gruner, *Electrodynamics of Solids* (Cambridge University Press, England, 2002).
[41] M. Nakajima, K. Yanase, F. Nabeshima, Y. Imai, A. Maeda, and S. Tajima, Phys. Rev. B **95**, 184502 (2017).
[42] I. Tsukada, M. Hanawa, S. Komiya, T. Akiike, R. Tanaka, Y. Imai, and A. Maeda, Phys. Rev. B **81**, 054515 (2010).